BAU Journal - Science and Technology

Volume 2 | Issue 2
ISSN: 2706-784X

Article 2

June 2021

AN IMPROVEMENT OF CROSS ENTROPY THRESHOLDING FOR SKIN CANCER

Nancy Aref Zreika N, A. Zreika
PhD Candidate , Faculty of Science , Beirut Arab University, Beirut, Lebanon, nancy_zreika@hotmail.com

Ali El Zaart
Professor, Faculty of Science, Beirut Arab University, Beirut, Lebanon, elzaart@bau.edu.lb

Abdallah Al Shakik
Associate Professor, Faculty of Science, Beirut Arab University, Beirut, Lebanon, a.alshakik@bau.edu.lb

AN IMPROVEMENT OF CROSS ENTROPY THRESHOLDING FOR SKIN CANCER

Abstract

Image processing procedures in medical diagnosis are used to improve diagnosis accuracy. An example of this is skin cancer detection using the thresholding approach. Thus, research studies involved in identification of inherited mutations predisposing family members to malignant melanoma have been performed in the Cancer Genetics field. Melanoma is one of the deadliest cancers, but could be cured when diagnosed early. A fundamental step in image processing is segmentation that includes thresholding, among others. Thresholding is based on finding the optimal thresholds value that partitions the image into multiple classes to be able to distinguish the objects from the background. The algorithm developed in this work is based on Minimum Cross Entropy Thresholding (MCET) method, using statistical distributions. We improved the previous work of Pal by using separately different statistical distributions (Gaussian, Lognormal and Gamma) instead of Poisson distribution. We applied our improved methods on bimodal skin cancer images and obtained promising experimental results. The resulting segmented skin cancer images, using Gamma distribution yielded better estimation of the optimal threshold than does the same MCET method with Lognormal, Gaussian and Poisson distribution.

Keywords

Image Thresholding, Minimum Cross Entropy, Melanoma, Skin Images, Gamma, Gaussian, Log Normal and Poisson distributions, Bimodal technique

1. INTRODUCTION

Skin cancer is the most common type of cancers in humans [11]. Five main ABCDE properties (Asymmetry, Border, Color, Diameter, and Evolving) in the lesion are examined to rule out skin cancer [12]. Diagnosis by physicians is helped by several image analysis techniques to measure these properties [9]. Accurate analysis of the lesion in the image should be distinguished from the background and its boundaries. This is done by several image segmentation techniques that identify the boundaries of a lesion, by exploiting the color and the texture characteristics in an image [13]. A fundamental step in image analysis is image segmentation that precedes feature extraction, selection and classification. Broadly, there are four classes of segmentation methods, including edge-based methods, region-based methods, thresholding-based methods, and hybrid methods [20,21]. Edge-based methods spotlight around contour detection. Segmentation is performed by finding contour of each object within an image. In region-based methods, the main idea is to estimate for each pixel which classes it belongs to. Thresholding-based methods are well-known and most popular for image segmentation. Thresholding consists in converting a multi-level image into a binary image. It is based on the assumption that the foreground and the background in the image have two distinct gray level distributions [2]. Segmentation is performed by finding threshold values, which are separating between gray level distributions of foreground and its background. The regions having gray levels below the threshold are assigned to the background and the regions having gray levels above the threshold are assigned to the objects, or vice versa [10]. Hybrid methods offer a solution to the problems of the previous methods by combining two or more of these methods to complement weaknesses in each other [24]. It yields high precision, accuracy and efficiency of segmented images.

For image segmentation, thresholding is related to thresholds estimation problem [1]. Finding a threshold value that partitions or clusters the gray-level values of the image into two classes, one representing the object while the other representing the background, is one of the aims of thresholding techniques.

Section 2 explains the cross entropy thresholding. In section 3, we introduced the four statistical distributions, their chart and their properties. Section 4 describes our proposed improvement Method of PAL and its algorithm. Section 5 explains the performance measures. Section 6 includes experimental results of the applying method. Finally, we stated our conclusion.

2. ENTROPY BASED THRESHOLDING

Kullback has proposed the Cross Entropy, to measure the theoretic information distance between two distributions. The minimization of the cross entropy forces the total intensity in the thresholded image to be identical to that of the original image in both the object and the background regions. The more similar the distribution of two variables, the smaller cross entropy is, and vice versa.

The cross entropy is defined as [4]: $$D(F, G)= \sum_{i=0}^{L} f_i . log \frac{f_i}{g_i} \qquad (1)$$

where, F and G are two different sources of information, f_i and g_i are the two statistical distributions of the two sources while L refers to the number of information values.

To determine the optimal threshold t^* of an image I, Minimum Cross Entropy Thresholding technique (MCET) minimizes the cross entropy between original image I and the resulting thresholded image I_t. Once the optimal threshold is determined, pixels are classified into two classes: C1 = {0, 1, …, t-1} and C2 = {t, t+1, …, L-1} where C1 is the class of pixels which fall below the optimal threshold, and C2 is the class of pixels which are equal or exceed the optimal threshold. C1 represents the object class and C2 represents the background class. Given the threshold t of an image I whose pixels are represented by the function $I(x, y)$, the resulting thresholded image I_t is defined as:

$$I_t(x,y)= \begin{cases} 0, & I(x,y) < t \\ 1, & I(x,y) \geq t \end{cases} \qquad (2)$$

Entropy based thresholding considers an image histogram as a probability distribution and then selects an optimal threshold value to separate object from the background [8]. Figure 1 shows an example of a histogram with the threshold line separating the object class from the background class.

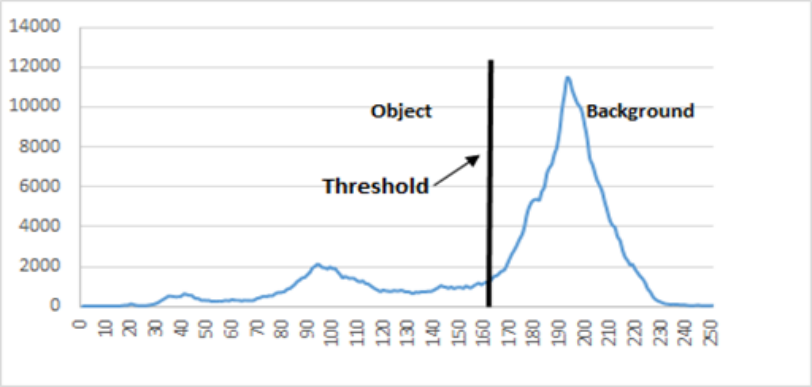

Fig.1**:** An example of a histogram with the threshold line separating the object class from the background class.

Li and Lee estimate the threshold by using the cross entropy defined by Kullback.
According to Entropy-Li and Lee, the cross entropy *D (I, I_t)* between the original image *(I)* and the thresholded image *(I_t)* is defined as:

$$D(I, I_t) = \sum_{i=0}^{t} i.h(i).log\frac{i}{\mu_O} + \sum_{i=t+1}^{L} i.h(i).log\frac{i}{\mu_B} \quad (3)$$

Where *i* counts from 1 till L, *h(i)* is the histogram of the original image, *t* is the threshold of the image, and μ_O and μ_B are the mean value of object and background regions in the original image.
However, the objective function of Kullback is a non-symmetric function therefore, it cannot be called divergence. To overcome this problem, Brink and Pendock proposed a new method based on a true symmetric cross entropy and they redefined the information theoretic distance as:

$$D(F, G) = \sum_{i=0}^{L} f_i . log\frac{f_i}{g_i} + \sum_{i=0}^{L} g_i . log\frac{g_i}{f_i} \quad (4)$$

Exhaustively, the cross entropy for the object and background regions are respectively $D_O(t)$ and $D_B(t)$:

$$D_O(t) = D(F_O, G_O) = \sum_{i=0}^{t} f_i^o \, log\left(\frac{f_i^o}{g_i^o}\right) + \sum_{i=0}^{t} g_i^o \, log\left(\frac{g_i^o}{f_i^o}\right) \quad (5)$$

$$D_B(t) = D(F_B, G_B) = \sum_{i=t+1}^{L-1} f_i^B \, log\left(\frac{f_i^B}{g_i^B}\right) + \sum_{i=t+1}^{L-1} g_i^B \, log\left(\frac{g_i^B}{f_i^B}\right) \quad (6)$$

Thus, the total cross entropy is: $D(t) = D_O(t) + D_B(t)$ (7)
and the cross entropy *D (I, I_t)* between the original image *(I)* and the thresholded image *(I_t)* becomes:

$$D(I, I_t) = \sum_{i=0}^{t} i.h(i).log\frac{i}{\mu_O} + \sum_{i=t+1}^{L} i.h(i).log\frac{i}{\mu_B} + \sum_{i=0}^{t} \mu_O.h(i).log\frac{\mu_O}{i} + \sum_{i=t+1}^{L} \mu_B.h(i).log\frac{\mu_B}{i} \quad (8)$$

Both Lee and Brink assumed that each pixel in the object and the background of the thresholded image should be equal to the average of pixels' value respectively in the corresponding partition of the original image. Wherever, Pal assumed that each pixel in the segmented image is modeled by a statistical distribution [9]. In his view, the gray values in the object region and the background region follow the Poisson distribution (respectively $g_i^O = \frac{e^{-\mu_O}}{i!}\mu_O^i$ and $g_i^B = \frac{e^{-\mu_B}}{i!}\mu_B^i$), and he used the symmetric version of distance defined by Brink and Pendock in the equations (5), (6) and (7), to develop a cross entropy method that is more general than Li and Brink [11].
To improve the work of Pal, we propose in this paper to use others statistical distributions that are more general than Poisson distribution, therefore, we estimate the optimal threshold by using Pal-MCET method with separately Gaussian, Lognormal and Gamma distributions.

3. STATISTICAL DISTRIBUTIONS

A histogram represents statistical information for image pixels. In a histogram, the number of pixels at each gray level or color intensity level (pixels intensity distribution), are graphed. Essentially, there are two types of distributions of gray level (mode): symmetric and non-symmetric. Poisson and Gaussian can approximate only a symmetric shape of histogram whereas Log Normal and Gamma distributions represent both symmetric and non-symmetric modes. Next, we introduce a general description of the statistical distributions used in our literature.

3.1. Poisson Distribution

In probability theory, a Poisson distribution is a discrete probability distribution that is used for discrete data. Poisson can only approximate a symmetric shape of the histogram. The probability density function of the Poisson distribution is:

$$f = \frac{e^{-\mu}}{i!}\mu^{i} \qquad (9)$$

Where μ is the mean value of the image, and is computed as [9]:

$$\mu = \frac{\sum_{i=0}^{L} i.h(i)}{\sum_{i=0}^{L} h(i)} \qquad (10)$$

Figure 2 shows the Poisson distribution with different means. It is clear that Poisson can approximate only a symmetric data.

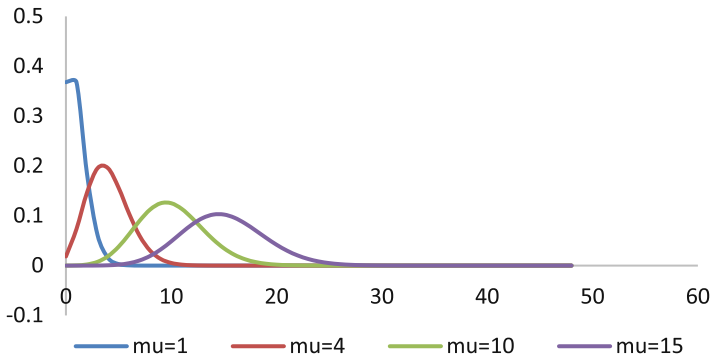

Fig.2: Poisson Distribution with different means
Reference: N. Zreika.

3.2. Gaussian Distribution

In probability theory, Gaussian distribution is a continuous probability distribution and has a bell-shaped probability density function, known as the Gaussian function [16]:

$$f(x,\mu,\sigma) = \frac{1}{\sigma\sqrt{2\pi}} e^{\frac{-1}{2}\left(\frac{x-\mu}{\sigma}\right)^{2}} \qquad (11)$$

Where x is the pixel's intensity level; σ is the standard deviation and μ is the mean.
Gaussian distribution can only approximate a symmetric shape of the histogram. Figure 2, shows a Gaussian Distribution with same value of mean μ and different standard deviation σ. Therefore, the mean μ and the standard deviation σ can be estimated as following [9]:

$$\mu = \frac{\sum_{i=0}^{L} i.h(i)}{\sum_{i=0}^{L} h(i)} \qquad (12)$$

$$\sigma^{2} = \frac{\sum_{i=0}^{L} (i-\mu)^{2}.h(i)}{\sum_{i=0}^{L} h(i)} \qquad (13)$$

Figure 3 shows the Gaussian distribution with same value of mean μ and different value of standard deviation σ. It is clear that Gaussian distribution can approximate only a symmetric shape of histogram.

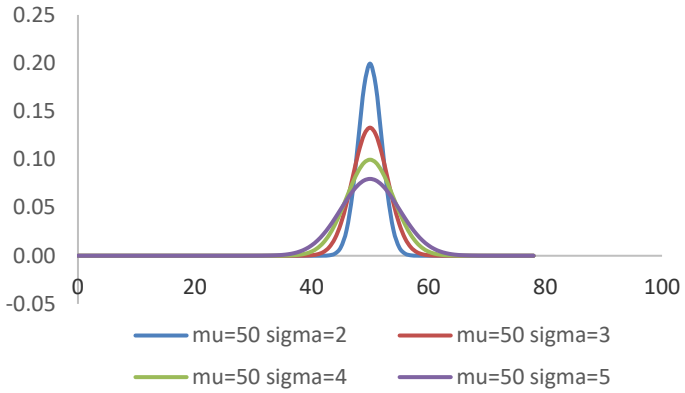

Fig.3: Gaussian Distribution with same value of mean μ and different value of standard deviation σ.
Reference: N. Zreika.

3.3. Log Normal Distribution

Log-normal distribution is a continuous probability distribution of a random variable whose logarithm is normally distributed [9,10]. Log-Normal distribution is used to model symmetric and moderate positively skewed data. The probability density function of the Lognormal distribution is defined as [15]:

$$f(x,\mu,\sigma) = \frac{1}{x\sigma\sqrt{2\pi}} e^{\frac{-1}{2}\left(\frac{lnx-\mu}{\sigma}\right)^2} \qquad (14)$$

Where x is the pixel's intensity level; μ is the mean and σ is the standard deviation. μ and σ are estimated as following:

$$\mu = \frac{\sum_{i=0}^{L} ln(i).h(i)}{\sum_{i=0}^{L} h(i)} \qquad (15)$$

$$\sigma^2 = \frac{\sum_{i=0}^{L} (ln(i)-\mu)^2.h(i)}{\sum_{i=0}^{L} h(i)} \qquad (16)$$

Figure 4 shows the Lognormal distribution with same value of mean μ and different value of standard deviation σ. we can see that if σ= 0.1, the distribution is symmetric. As σ increases, the distribution tends to be skewed to right.

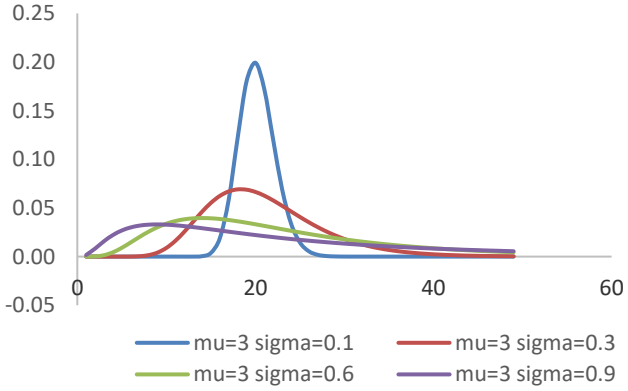

Fig.4: Log Normal Distribution with same mean and different value of standard deviation σ.
Reference: N. Zreika.

3.4. Gamma Distribution

Gamma Distribution is a two parameter family of continuous probability distributions in probability theory and statistics. It is a general type of statistical distribution. When simplicity and capability to provide symmetric and non-symmetric histograms are sought, Gamma distribution is used [20]. By changing the parameter shape N, the shape of Gamma distribution function can be altered from symmetric to asymmetric. The probability density function of the Gamma distribution in homogenous area is given by [6,7]:

$$f(x,\mu,N) = \frac{2q}{\mu}\frac{N^N}{\Gamma(N)}\left(\frac{qx}{\mu}\right)^{2N-1} e^{-N\left(\frac{qx}{\mu}\right)^2} \qquad (17)$$

Where $q = \frac{\Gamma(N+0.5)}{\sqrt{N}\,\Gamma(N)}$, x is the intensity of the pixel, μ is the mean value of the distribution and *N* is the shape of distribution. the mean μ is estimated as following:

$$\mu^2 = \frac{\sum_{i=0}^{L} h(i).i^2.q^2}{\sum_{i=0}^{L} h(i)} \qquad (18)$$

Figure 5 shows the Gamma distribution for one mode and with different shape parameter N and same mean μ = 10. In this Figure, we can see that if N =1, the distribution is skewed to right. As N increases, the distribution tends to be symmetric.

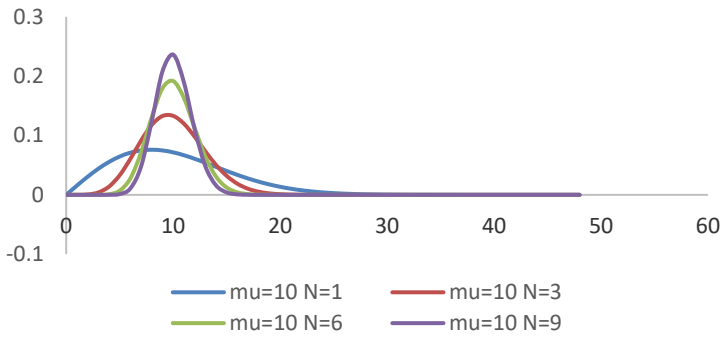

Fig.5: Gamma Distribution with same mean and different value shape parameter N.
Reference: N. Zreika.

Many algorithms have been proposed for cross entropy thresholding. Li and Lee (1993) have introduced the minimum cross entropy thresholding algorithm that selects the threshold, which minimizes the cross entropy between the segmented image and the original image [1]. They used the kullback's information theoretic distance D between two probability distributions [3,4], and they proposed a sequential method based on Gaussian distribution [6].

An iterative method derived from Li and Lee [5] has been developed by Li and Tam (1998). These authors find the threshold value by minimizing the cross entropy using Gaussian distribution [5]. Also, they found the optimal threshold value by minimizing cross entropy using Gamma distribution [7].

Al-Attas and El-Zaart (2006) proposed two sequential methods, one derived from Li and Lee [1] and another derived from Li and Tam [5] for finding optimal threshold value by minimizing Cross Entropy using Gamma distribution to describe data in images. Al-Osaimi and El-Zaart (2008) developed a new iterative algorithm derived from Li and Lee [10] and another derived from Li and Tam [2] to find the optimal threshold value by minimizing cross entropy using Gamma distribution [5].

4. THE PROPOSED IMPROVEMENT OF PAL METHOD

As stated before, Pal assumed that image histograms are modeled by a Poisson distribution [9]. He used the probability density function of Poisson distribution to estimate the distribution of gray level in the object and the background of the thresholded image (respectively $g^O = \frac{e^{-\mu_O}}{i!}\mu_O^i$ and $g^B = \frac{e^{-\mu_B}}{i!}\mu_B^i$), as well he estimated the mean value of object and background regions (respectively μ_O and μ_B) based on Gaussian distribution.

However, the data in an image does not always follow Poisson distribution. In general, Poisson distribution can only approximate a symmetric shape of the histogram but sometimes the histogram of an image is not symmetric, or it could be positively skewed. In this case, a more general distribution to represent the data of the image is required. In this paper, our goal is to propose an improvement of Pal method and El-Zaart method by using statistical distributions other than Poisson and comparing them with Pal Poisson. We used Gaussian distribution [7] which can model only symmetric data. We also used Gamma distribution [7] which can model symmetric and skewed to the right data, as well as Lognormal distribution which can model moderate positively skewed data and symmetric data.

Figure 7 shows the evolution of Pal Method and the proposed improvement made by N. Zreika & El-Zaart.

The sequential algorithm for our proposed improvement method of Pal using separately the 4 described statistical distributions is described as follows:

1. Input: image *I (x, y)*
2. Compute histogram *h(i)* of the input image, where *i=0…255.*
3. For each value of threshold *t=1, ..., 255*

3.1 Compute $\mu_O(t)$ and $\mu_B(t)$ using one of the statistical distributions above.
3.2 Compute the probability distributions of the object and background regions in the segmented image g_i^o and g_i^B.
3.3 Compute $D_O(t)$ and $D_B(t)$ using equations (5) and (6).
3.4 Compute the total cross entropy using equation (7).
$D(t) = D_O(t) + D_B(t)$.
3.5 Compute the minimum distance and the corresponding threshold

```
If (min > D(t))
        {
    min = D(t) ;
        }
```

4. Output: optimal threshold: t^*

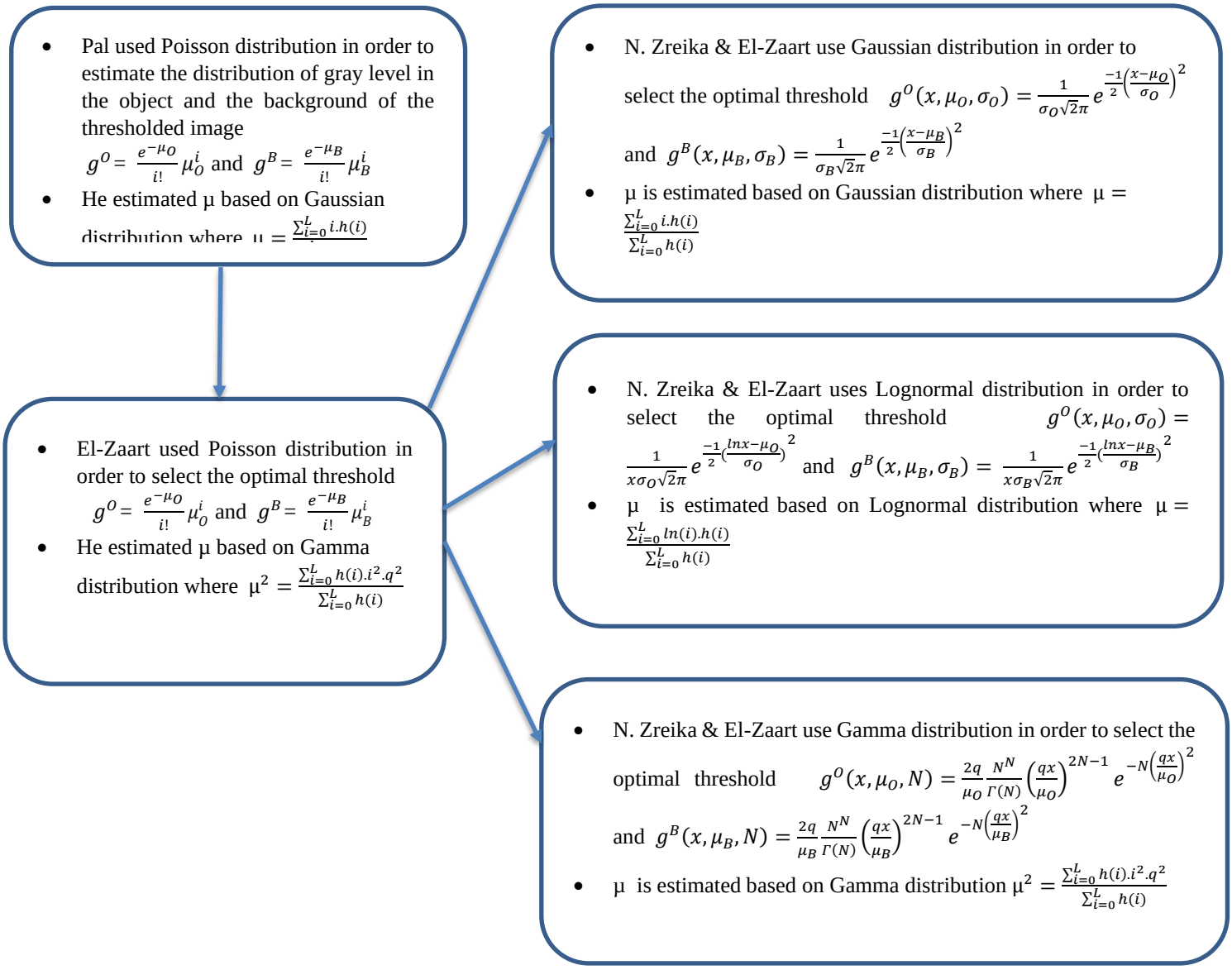

Fig.7: Evolution of Pal Method

5. PERFORMANCE MEASURES

The quality of the segmentation result is quantitatively evaluated based on two performance measures: Image Uniformity (UN) and Region Contrast (RC) [10]. We have also calculated the arithmetic average of the normalized score of UN and RC represented by AVG.

Image Uniformity is generally used to describe region homogeneity in an image. It is proportional to the variances of the two classes (foreground and background). It is based on the assumption that a good threshold value will classify pixels in an image to foreground and background classes where variances in both classes are minimized. For a given threshold *t*, image uniformity is defined by [10]:

$$UN(t) = 1 - \frac{\sigma_O^2(t)+\sigma_B^2(t)}{C} \qquad (19)$$

where $\sigma_O^2(t)$ and $\sigma_B^2(t)$ represent respectively the variance of the foreground and background regions, and

$$C = \frac{(g_{max} - g_{min})^2}{2} \quad (20)$$

Where g_{max} and g_{min} are respectively the maximum and minimum grey levels values in the original image.

g_{max} and g_{min} ranges between [0, L].

The value of UN ranges between [0,1], where a value of 1 means that the segmentation is perfect while a value of 0 means that the segmentation is bad.

Region Contrast (RC) is used to detect if the segmented image has high contrast across adjacent regions. The higher the contrast across adjacent regions, the better the quality of the segmented image. For a given threshold t, the region contrast is defined as [10]:

$$RC(t) = \frac{|\mu_O(t) - \mu_B(t)|}{\mu_O(t) + \mu_B(t)} \quad (21)$$

Where μ_O and μ_B are respectively the average of the gray level values of the object and the background classes. Similar to UN, the value of RC ranges between [0,1], where a value of 1 means that the segmentation is perfect while a value of 0 means that the segmentation is bad.

6. EXPERIMENTAL RESULTS AND DISCUSSION

An algorithm was implemented based on our new proposed distributions (Gaussian, Log Normal and Gamma), and tested on a set of 200 images. The images were taken from patients with potential skin cancer [22]. In addition, we implemented the original Pal's Poisson method for comparison purposes. Our objective was to prove which distribution yields better segmentation for skin cancer images.

Table 1 shows the results of images after applying the 3 proposed improvement methods on our dataset. We selected the images where all the methods give a good segmentation. The table lists the threshold found as well as the 3 performance measures UN, RC, and AVG with their rank. For each image, the methods were then ranked according to their performance. Promising results and a better estimation of the optimal threshold value have been obtained from MCET-Gamma (Table 2). Thus, 80% of tested images had better segmentation results with Gamma method. This was based on the average performance metric of uniformity and inter-region contrast. In 85% of the cases inter-region contrast was higher with MCET-Gamma thresholding results while for uniformity measure, MCET-Poisson was ranked 1st in 69% of the images.

In conclusion, we propose that using MCET-Gamma results in better segmentation of skin cancer images than using the other methods. Doing this, skin cancer images follow a gamma distribution rather than Poisson, Gaussian or Lognormal distribution.

The following figures (Figure 8, Figure 9, Figure 10 and Figure 11) show a sample of the testing results. Each figure contains the original image (a), its grayscale version (b), the thresholded images respectively resulting from MCET-Poisson (c), MCET-Gaussian (d), MCET- Log Normal (e), and MCET- Gamma (f). The graph (g) shows the histogram of the image with 4 vertical lines representing the value of thresholds found in each method. Each figure also lists, for each method, the corresponding UN, RC and AVG values.

In Figure 8, according to UN measure, MCET-Poisson shows best segmentation results (UN = 0.9532), whereas according to RC and AVG measures, MCET-Gamma shows best segmentation results (RC = 0.4154, AVG = 0.6834).

In Figure 9, according to UN, RC and AVG measures, MCET-Poisson shows best segmentation results (UN = 0.9651, RC = 0.4065, AVG = 0.6799).

In Figure 10, according to UN measure, MCET-Poisson shows best segmentation results (UN = 0.9710), whereas according to RC and AVG measures, MCET-Gamma shows best segmentation results (RC = 0.4660, AVG = 0.7159).

In Figure 11, according to UN and AVG measures, MCET-Lognormal shows best segmentation results (UN = 0.9759, AVG=0.7045), whereas according to RC measure, MCET-Poisson shows best segmentation results (RC = 0.4338).

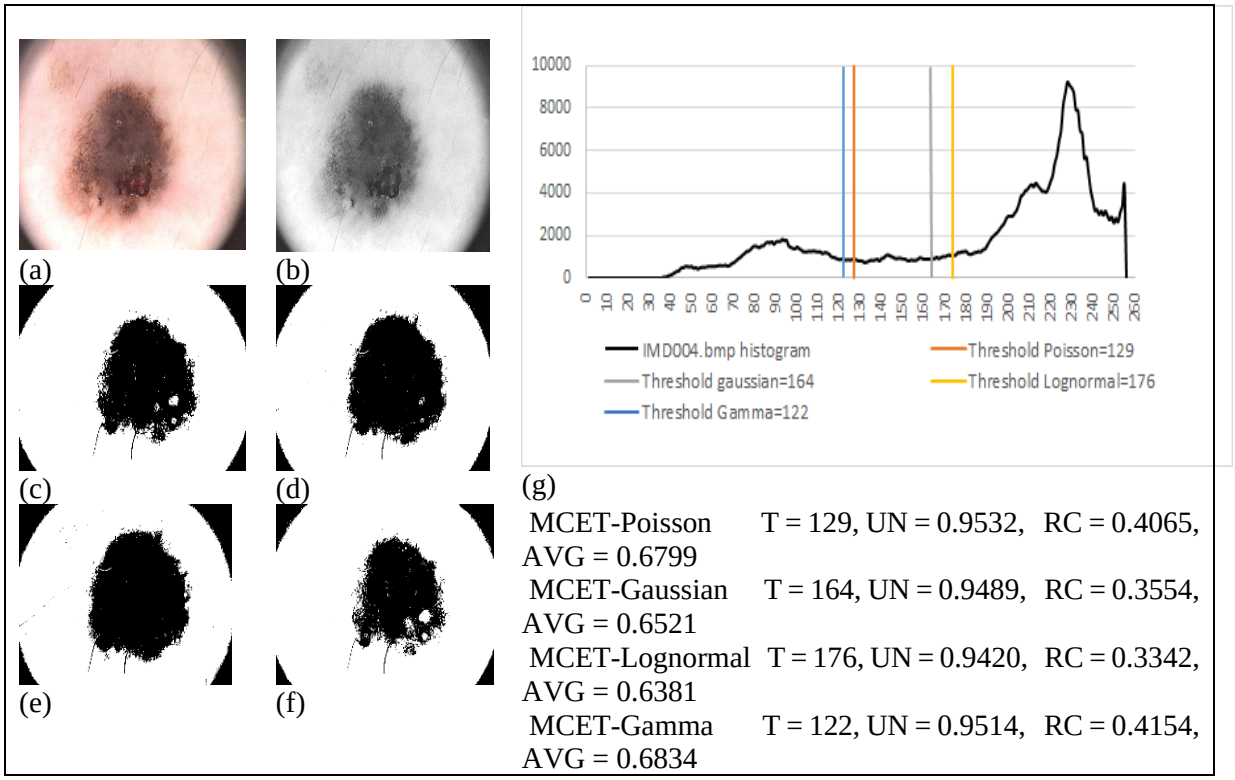

MCET-Poisson T = 129, UN = 0.9532, RC = 0.4065, AVG = 0.6799
MCET-Gaussian T = 164, UN = 0.9489, RC = 0.3554, AVG = 0.6521
MCET-Lognormal T = 176, UN = 0.9420, RC = 0.3342, AVG = 0.6381
MCET-Gamma T = 122, UN = 0.9514, RC = 0.4154, AVG = 0.6834

Fig.8 : (a)Original Image (IMD004). (b)Grayscale version. (c)Segmented Image using MCET-Poisson. (d)Segmented Image using MCET-Gaussian. (e)Segmented Image using MCET- Log Normal. (f) Segmented Image using MCET- Gamma. (g) Histogram of IMD004 image.

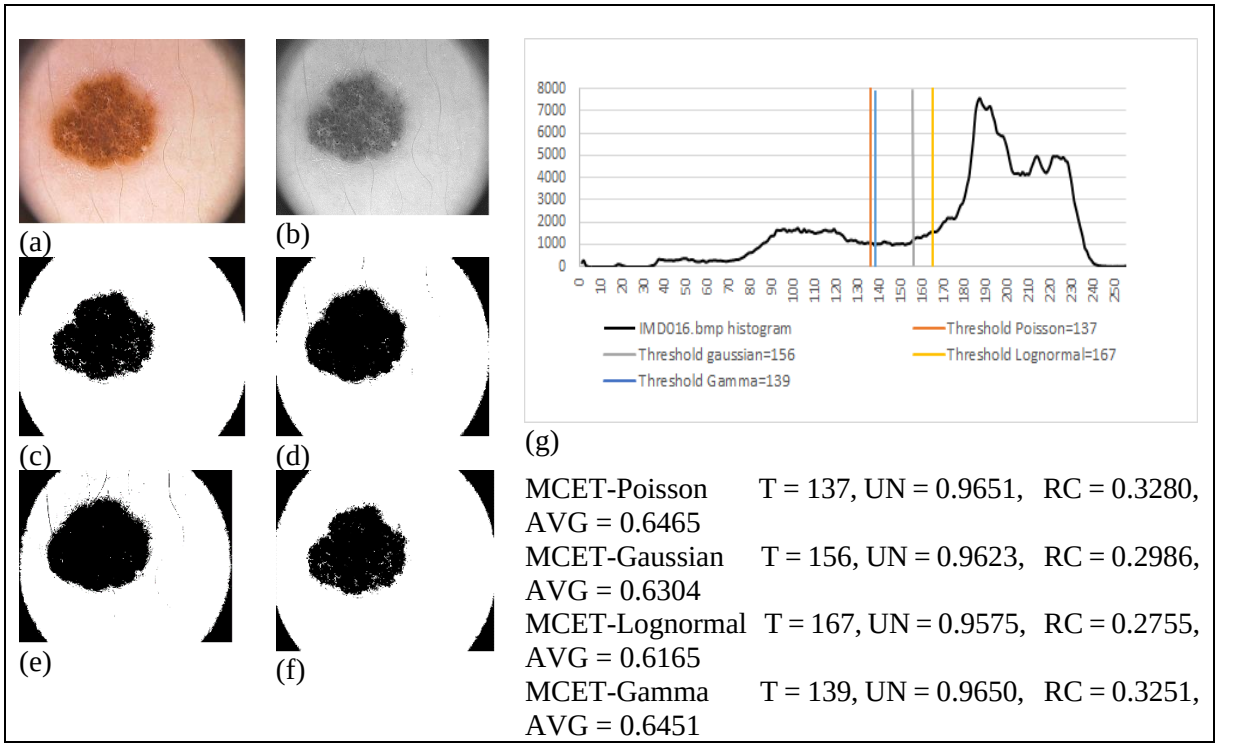

MCET-Poisson T = 137, UN = 0.9651, RC = 0.3280, AVG = 0.6465
MCET-Gaussian T = 156, UN = 0.9623, RC = 0.2986, AVG = 0.6304
MCET-Lognormal T = 167, UN = 0.9575, RC = 0.2755, AVG = 0.6165
MCET-Gamma T = 139, UN = 0.9650, RC = 0.3251, AVG = 0.6451

Fig.9: (a) Original Image (IMD016). (b)Grayscale version. (c)Segmented Image using MCET-Poisson. (d)Segmented Image using MCET-Gaussian. (e)Segmented Image using MCET- Log Normal. (f)Segmented Image using MCET- Gamma. (g) Histogram of IMD016 image. Reference: N. Zreika.

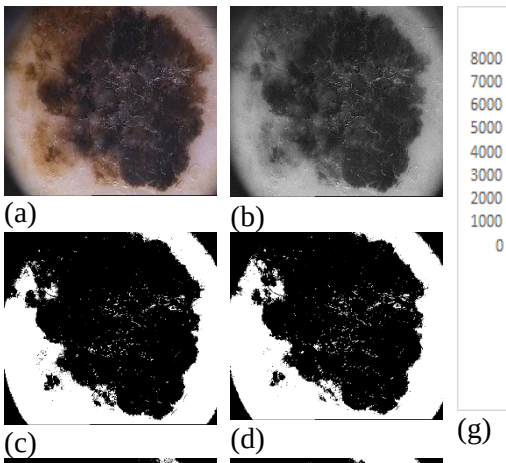

(a) (b)

(c) (d)

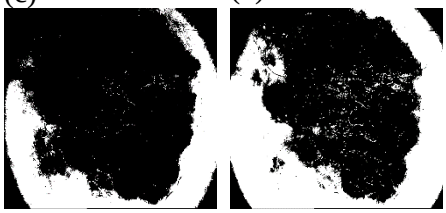

(e) (f)

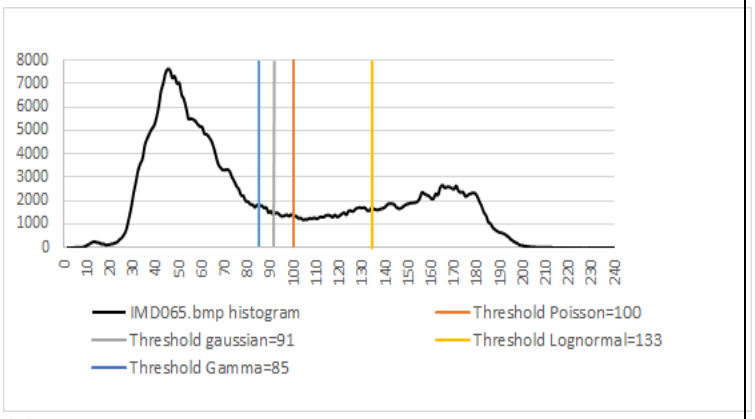

(g)

MCET-Poisson T = 100, UN = 0.9710, RC = 0.4608, AVG = 0.7159
MCET-Gaussian T = 91, UN = 0.9685, RC = 0.4644, AVG = 0.7164
MCET-Lognormal T = 133, UN = 0.9679, RC = 0.4331, AVG = 0.7005
MCET-Gamma T = 85, UN = 0.9659, RC = 0.4660, AVG = 0.7159

Fig.10 : (a)Original Image (IMD065). (b)Grayscale version. (c)Segmented Image using MCET-Poisson. (d)Segmented Image using MCET-Gaussian. (e)Segmented Image using MCET- Log Normal. (f) Segmented Image using MCET-Gamma. (g) Histogram of IMD065 image.

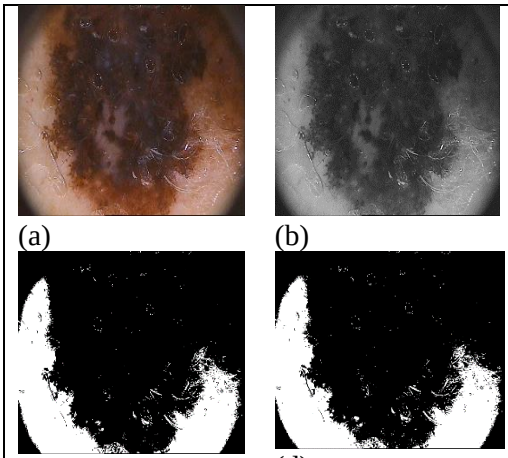

(a) (b)

(c) (d)

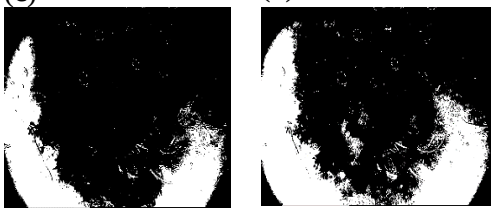

(e) (f)

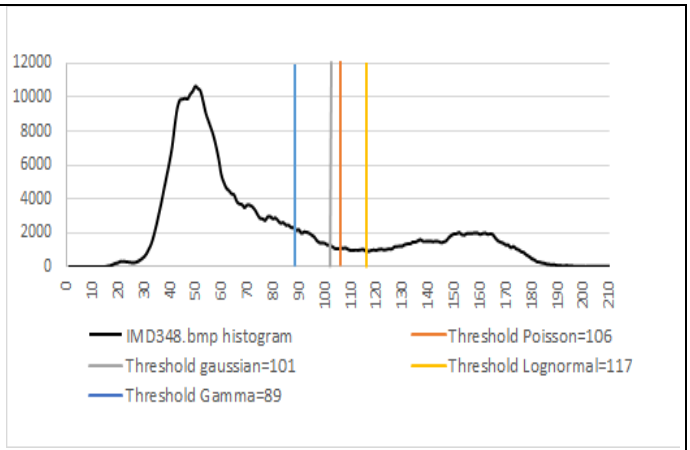

(g)

MCET-Poisson T = 106, UN = 0.9751, RC = 0.4338, AVG = 0.7044
MCET-Gaussian T = 101, UN = 0.9740, RC = 0.4333, AVG = 0.7036
MCET-Lognormal T = 117, UN = 0.9759, RC = 0.4331, AVG = 0.7045
MCET-Gamma T = 89, UN = 0.9687, RC = 0.4289, AVG = 0.6988

Fig.11 : (a)Original Image (IMD348). (b)Grayscale version. (c)Segmented Image using MCET-Poisson. (d)Segmented Image using MCET-Gaussian. (e)Segmented Image using MCET- Log Normal. (f) Segmented Image using MCET-Gamma. (g) Histogram of IMD348 image. Reference: N. Zreika.

Table 1: Comparison of Performance Measures (UN, RC, and AVR) between MCET-Poisson, MCET-Gaussian, MCET-Lognormal and MCET-Gamma, Reference: N. Zreika.

	Distribution	**Threshold**	**UN**	**UN/Rank**	**RC**	**RC/Rank**	**AVG**	**AVG/Rank**
IMD002	Poisson	116	0.9677	1	0.3452	2	0.6565	2
	Gaussian	132	0.9671	2	0.3249	3	0.6460	3
	Lognormal	142	0.9636	4	0.3074	4	0.6355	4
	Gamma	106	0.9648	3	0.3599	1	0.6624	1
IMD003	Poisson	134	0.9545	1	0.3189	2	0.6367	2
	Gaussian	153	0.9522	3	0.2782	3	0.6152	3
	Lognormal	158	0.9510	4	0.2682	4	0.6096	4
	Gamma	132	0.9544	2	0.3231	1	0.6387	1
IMD004	Poisson	129	0.9532	1	0.4065	2	0.6799	2
	Gaussian	164	0.9489	3	0.3554	3	0.6521	3
	Lognormal	176	0.9420	4	0.3342	4	0.6381	4
	Gamma	122	0.9514	2	0.4154	1	0.6834	1
IMD015	Poisson	127	0.9777	1	0.3421	2	0.6599	2
	Gaussian	144	0.9763	3	0.3234	3	0.6499	3
	Lognormal	169	0.9632	4	0.2758	4	0.6195	4
	Gamma	125	0.9776	2	0.3439	1	0.6608	1
IMD016	Poisson	137	0.9651	1	0.3280	1	0.6465	1
	Gaussian	156	0.9623	3	0.2986	3	0.6304	3
	Lognormal	167	0.9575	4	0.2755	4	0.6165	4
	Gamma	139	0.9650	2	0.3251	2	0.6451	2
IMD017	Poisson	124	0.9628	2	0.3671	2	0.6649	2
	Gaussian	127	0.9633	1	0.3647	3	0.6640	3
	Lognormal	151	0.9612	3	0.3415	4	0.6514	4
	Gamma	112	0.9583	4	0.3763	1	0.6673	1
IMD021	Poisson	99	0.9744	1	0.3739	2	0.6741	2
	Gaussian	119	0.9709	3	0.3409	3	0.6559	3
	Lognormal	127	0.9670	4	0.3253	4	0.6462	4
	Gamma	97	0.9742	2	0.3770	1	0.6756	1
IMD027	Poisson	150	0.9696	1	0.2752	2	0.6224	2
	Gaussian	169	0.9669	3	0.2485	3	0.6077	3
	Lognormal	179	0.9627	4	0.2300	4	0.5963	4
	Gamma	149	0.9695	2	0.2765	1	0.6230	1
IMD031	Poisson	143	0.9724	2	0.3356	2	0.6540	1
	Gaussian	133	0.9697	3	0.3357	1	0.6527	3
	Lognormal	153	0.9732	1	0.3337	4	0.6534	2
	Gamma	129	0.9678	4	0.3352	3	0.6515	4
IMD038	Poisson	108	0.9705	1	0.4132	2	0.6918	2
	Gaussian	145	0.9645	3	0.3477	3	0.6561	3
	Lognormal	153	0.9603	4	0.3310	4	0.6456	4
	Gamma	104	0.9698	2	0.4211	1	0.6954	1
IMD041	Poisson	134	0.9619	1	0.3645	2	0.6632	2
	Gaussian	154	0.9606	3	0.3403	3	0.6504	3
	Lognormal	169	0.9547	4	0.3185	4	0.6366	4
	Gamma	132	0.9617	2	0.3663	1	0.6640	1
IMD042	Poisson	104	0.9706	2	0.3960	2	0.6833	2
	Gaussian	105	0.9708	1	0.3947	3	0.6828	3
	Lognormal	126	0.9700	3	0.3664	4	0.6682	4
	Gamma	98	0.9693	4	0.4026	1	0.6859	1
IMD043	Poisson	95	0.9688	2	0.3920	2	0.6804	2
	Gaussian	102	0.9691	1	0.3797	3	0.6744	3
	Lognormal	112	0.9680	3	0.3599	4	0.6639	4
	Gamma	90	0.9679	4	0.4016	1	0.6847	1
IMD047	Poisson	105	0.9677	1	0.3245	2	0.6461	2
	Gaussian	119	0.9658	3	0.2996	3	0.6327	3
	Lognormal	126	0.9624	4	0.2820	4	0.6222	4
	Gamma	100	0.9670	2	0.3321	1	0.6496	1
IMD049	Poisson	113	0.9762	1	0.3665	2	0.6714	2

	Gaussian	131	0.9742	3	0.3406	3	0.6574	3
	Lognormal	145	0.9683	4	0.3100	4	0.6392	4
	Gamma	108	0.9757	2	0.3725	1	0.6741	1
IMD057	Poisson	110	0.9763	1	0.4163	3	0.6963	3
	Gaussian	101	0.9739	3	0.4216	2	0.6977	2
	Lognormal	135	0.9751	2	0.3947	4	0.6849	4
	Gamma	98	0.9728	4	0.4229	1	0.6979	1
IMD058	Poisson	116	0.9838	2	0.2700	2	0.6269	1
	Gaussian	123	0.9840	1	0.2677	3	0.6258	3
	Lognormal		0.9824	3	0.2610	4	0.6217	4
	Gamma	106	0.9819	4	0.2717	1	0.6268	2
IMD063	Poisson	105	0.9814	2	0.3654	2	0.6734	2
	Gaussian	116	0.9816	1	0.3567	3	0.6691	3
	Lognormal	132	0.9775	4	0.3359	4	0.6567	4
	Gamma	92	0.9779	3	0.3734	1	0.6757	1
IMD065	Poisson	100	0.9710	1	0.4608	3	0.7159	2
	Gaussian	91	0.9685	2	0.4644	2	0.7164	1
	Lognormal	133	0.9679	3	0.4331	4	0.7005	3
	Gamma	85	0.9659	4	0.4660	1	0.7159	2
IMD075	Poisson	95	0.9768	1	0.4216	2	0.6992	2
	Gaussian	112	0.9760	2	0.3933	3	0.6847	3
	Lognormal	134	0.9672	4	0.3375	4	0.6524	4
	Gamma	89	134	3	0.4320	1	0.7039	1
IMD078	Poisson	130	0.9616	1	0.4084	2	0.6850	2
	Gaussian	160	0.9570	3	0.3695	3	0.6632	3
	Lognormal	182	0.9422	4	0.3278	4	0.6350	4
	Gamma	124	0.9606	2	0.4141	1	0.6873	1
IMD088	Poisson	116	0.9727	2	0.3335	2	0.6531	2
	Gaussian	117	0.9728	1	0.3327	3	0.6528	3
	Lognormal	152	0.9631	4	0.2879	4	0.6255	4
	Gamma	108	0.9719	3	0.3389	1	0.6554	1
IMD140	Poisson	90	0.9643	1	0.4908	2	0.7275	2
	Gaussian	134	0.9570	3	0.3885	3	0.6728	3
	Lognormal	140	0.9538	4	0.3733	4	0.6636	4
	Gamma	82	0.9623	2	0.5092	1	0.7358	1
IMD149	Poisson	126	0.9678	2	0.3601	2	0.6640	2
	Gaussian	136	0.9681	1	0.3524	3	0.6602	3
	Lognormal	152	0.9646	4	0.3344	4	0.6495	4
	Gamma	117	0.9657	3	0.3673	1	0.6665	1
IMD150	Poisson	150	0.9538	1	0.3922	2	0.6730	2
	Gaussian	187	0.9490	3	0.3573	3	0.6532	3
	Lognormal	202	0.9403	4	0.3391	4	0.6397	4
	Gamma	138	0.9501	2	0.4021	1	0.6761	1
IMD169	Poisson	99	0.9804	2	0.4054	2	0.6929	2
	Gaussian	114	0.9805	1	0.3881	3	0.6843	3
	Lognormal	129	0.9766	4	0.3635	4	0.6701	4
	Gamma	91	0.9786	3	0.4145	1	0.6966	1
IMD171	Poisson	78	0.9749	1	0.4781	2	0.7265	2
	Gaussian	97	0.9748	2	0.4436	3	0.7092	3
	Lognormal	112	0.9699	4	0.4104	4	0.6901	4
	Gamma	70	0.9724	3	0.4951	1	0.7338	1
IMD173	Poisson	135	0.9686	2	0.3227	1	0.6456	1
	Gaussian	155	0.9657	3	0.2941	3	0.6299	3
	Lognormal	169	0.9588	4	0.2653	4	0.6121	4
	Gamma	137	0.9687	1	0.3201	2	0.6444	2
IMD197	Poisson	145	0.9543	1	0.3487	2	0.6515	2
	Gaussian	169	0.9516	3	0.3175	3	0.6345	3
	Lognormal	182	0.9448	4	0.2933	4	0.6190	4
	Gamma	141	0.9537	2	0.3551	1	0.6544	1
IMD211	Poisson	97	0.9786	2	0.3354	2	0.6570	2

	Gaussian	103	0.9789	1	0.3284	3	0.6537	3
	Lognormal	117	0.9756	4	0.3060	4	0.6408	4
	Gamma	93	0.9780	3	0.3393	1	0.6586	1
IMD348	Poisson	106	0.9751	2	0.4338	1	0.7044	2
	Gaussian	101	0.9740	3	0.4333	2	0.7036	3
	Lognormal	117	0.9759	1	0.4331	3	0.7045	1
	Gamma	89	0.9687	4	0.4289	4	0.6988	4
IMD419	Poisson	137	0.9778	2	0.3261	2	0.6520	2
	Gaussian	129	0.9760	3	0.3212	3	0.6486	3
	Lognormal	144	0.9785	1	0.3293	1	0.6539	1
	Gamma	119	0.9719	4	0.3117	4	0.6418	4

Table 2: Evaluation Of Performance Measures For The 4 Methods, Reference: N. Zreika.

	%UN	**%RC**	**%AVG**
MCET-Poisson	69%	11%	14%
MCET-Gaussian	18%	3%	3%
MCET-Lognormal	6%	1%	3%
MCET-Gamma	7%	85%	80%

7. CONCLUSION AND FUTURE WORK

We have compared three new variants MCET-Gamma, MCET-Lognormal, and MCET-Gaussian, with MCET-Poisson. The methods were tested on a dataset of skin cancer images [22]. Our experiments revealed that the optimal threshold can be found by using the Gamma Pal method rather than the traditional Poisson Pal method. In this regard, Gamma distribution is more general, and solves the problem of non-symmetric histograms in images.

In future work, we will apply our proposed methods on other datasets, and we will focus on extending these methods to a multi-level thresholding and heterogeneous thresholding.

REFERENCES

- Li, C. H., & Lee, C. K. (1993). Minimum cross entropy thresholding. *Pattern recognition*, *26*(4), 617-625.
- Gonzales, R. C., & Woods, R. E. (2008). Digital image processing 3rd ed.
- Ramac, L. C., & Varshney, P. K. (1997). Image thresholding based on Ali-Silvey distance measures. *Pattern Recognition*, *30*(7), 1161-1174.
- Kullback, S. (1997). *Information theory and statistics*. Courier Corporation.
- Li, C. H., & Tam, P. K. S. (1998). An iterative algorithm for minimum cross entropy thresholding. *Pattern recognition letters*, *19*(8), 771-776.
- Şengür, I. Türkoğlu And M. İnce (2006), "A Comparative Study On Entropic Thresholding Methods" *Journal of Electrical & Electronics Engineering*, vol.6, no. 2, pp. 183-188.
- Al-Attas, R., & El-Zaart, A. (2007). Thresholding of medical images using minimum cross entropy. In *3rd Kuala Lumpur International Conference on Biomedical Engineering 2006* (pp. 296-299). Springer, Berlin, Heidelberg.
- Brink, A. D., & Pendock, N. E. (1996). Minimum cross-entropy threshold selection. *Pattern recognition*, *29*(1), 179-188.
- Pal, N. (1996), "On Minimum cross entropy thresholding," *Pattern Recognition Letter*, vol. 29 no. 4, pp. 575–580.

- Sezgin, M., & Sankur, B. (2004). Survey over image thresholding techniques and quantitative performance evaluation. *Journal of Electronic imaging*, *13*(1), 146-165.
- Kopf, A. W., Salopek, T. G., Slade, J., Marghoob, A. A., & Bart, R. S. (1995). Techniques of cutaneous examination for the detection of skin cancer. *Cancer*, *75*(S2), 684-690.
- Pham, D. L. C. Xu, and J. L. Prince (2000), "A survey of current methods in medical image segmentation", *In Annual Review of Biomedical Engineering*, pp. 318–338.
- El-Zaart, A. (2006, February). Unsupervised Learning Technique for Image Segmentation. In *Proceedings of First National Information Technology Symposium* (pp. 205-210).
- Jambunathan, M. V. (1954). Some properties of beta and gamma distributions. *The annals of mathematical statistics*, 401-405.
- Forbes, C., Evans, M., Hastings, N., & Peacock, B. (2011). *Statistical distributions*. John Wiley & Sons.
- G.McPherson (1990),"Statistics in scientific investigation: its basis, application and interpretation", Springer-Verlag.
- A. El Zaart, A. Al-Mejrad and A. Saad (2004), "Segmentation of Mammography Images for Breast Cancer Detection", in the Proceedings of the Kuala Lumpur International Conference on Biomedical Engineering 2004 , pp. 225-228.
- Ferrari, R. J., Rangayyan, R. M., Borges, R. A., & Frere, A. F. (2004). Segmentation of the fibro-glandular disc in mammogrms using Gaussian mixture modelling. *Medical and Biological Engineering and Computing*, *42*(3), 378-387.
- Zreika, N. A., El Zaart, A., El Chakik, A., & El Arwadi, T. (2018, September). Skin Cancer Segmentation with Entropy PAL MCET using Gaussian Distribution. In *2018 4th International Conference on Applied and Theoretical Computing and Communication Technology (iCATccT)* (pp. 315-320). IEEE.
- El Zaart, A., Ziou, D., Wang, S., & Jiang, Q. (2002). Segmentation of SAR images. *Pattern Recognition*, *35*(3), 713-724.
- Zhang, J., Zheng, J., & Cai, J. (2010, June). A diffusion approach to seeded image segmentation. In *2010 IEEE Computer Society Conference on Computer Vision and Pattern Recognition* (pp. 2125-2132). IEEE.
- PH^2Database,https://www.fc.up.pt/addi/ph2%database.html, Accessed November 2017
- "Performance Evaluation" (2004), Journal of Electronic Imaging, vol. 13, no. 1, pp. 146-165
- Ritter, G., Wilson, J. (1990), "*Handbook of Computer Vision Algorithms in Image Algebra"*, CRC Press LLC, 1st Edition, ISBN: 0849326362.
- El-Zaart, A. (2015). Synthetic aperture radar images segmentation using minimum cross entropy with Gamma distribution. *International Journal of Signal and Image Processing*, *6*(4), 19-31.